Journal of Materials Chemistry B

Accepted Manuscript

ROYAL SOCIETY OF CHEMISTRY

www.rsc.org/materialsB

Journal Name

RSCPublishing

ARTICLE

Cite this: DOI: 10.1039/x0xx00000x

Received 00th January 2012,

Accepted 00th January 2012

DOI: 10.1039/x0xx00000x

www.rsc.org/

Self-assembled binary colloidal crystal monolayers as cell culture substrates

Peng-Yuan Wang[a,b], Hitesh Pingle[a], Peter Koegler[a,b], Helmut Thissen[b], and Peter Kingshott*[a]

This study investigated the formation of self-assembled binary colloidal crystal (BCC) monolayers using evaporation induced confined area assembly (EICAA), and fabricated a family of various BCCs for cell culture. A library of various BCCs with different structures was established and it was demonstrated that after stabilisation the BCCs have potential to be used as substrates with well-ordered surface topographies and chemistries for manipulating cell-surface interactions. Three cell types including MG63 osteoblasts, L929 fibroblasts, and primary human adipose-derived stem cells (hADSCs) show different responses on selected surfaces (either between BCCs or BCCs vs. flat controls). In general, cell spreading was inhibited on BCCs due to surface topography. Chemical composition presenting on the BCCs can compensate the topographic effect depending on what combination was used. The ordered topography and heterogeneous chemical patterns provide a complexity of the surface properties and have potential to be selectively modified with desired biomolecules for controlling of biointerface interactions.

1. Introduction

The control of mammalian cellular responses through surface chemistry and topography is important for both *in vitro* and *in vivo* biomedical applications, including cell culture tools, implantable medical devices, and regenerative medicine.[1] A number of studies have highlighted the importance of chemical and topographical patterns for influencing cellular behaviour,[2-4] where exploring the role of feature size and spacing, geometry, and order vs. disorder are exciting strategies to pursue. To date, photolithography and electron beam lithography (EBL), amongst others, are two common techniques used for generating chemical patterns and topographical features,[5] with their advantages being the ability to create precise geometries and patterns.[3] However, their disadvantages include the need for expensive equipment, time consuming procedures and the fact that often only relatively small surface areas are achievable, with lower resolution being the trade-off if larger areas are required.[6] Although pattern transfer techniques such as solvent-assisted micro-moulding (SAMIM) using poly(dimethyl siloxane) (PDMS) elastomers[7, 8] or nano-imprinting[9] have been widely used to reduce the cost and time for sample preparation, primary surfaces are often difficult to access. Furthermore, adding chemical patterns on topographic patterns need multiple steps with high complexity. We have developed an alternative approach that is potentially more economic and conceptually simpler and can yield a broad range of complex surface chemical and topographic patterns with high throughput.[10-13] It is based on self-assembled binary colloidal crystal layers, which allow precise control over surface features through careful choice of particle combinations and is thus an ideal alternative to fabricating advanced chemical patterns and surface topographies. Colloidal particles have been used as lithographic masks in colloidal lithography to control feature size and spacing using hexagonal close packed crystals made of different particle size.[6, 14] The versatility of the colloid based approach thus has a distinct advantage that allows biologists to explore cell-topography interactions on various length scales, with potentially high throughput.

Although the formation of colloidal crystal layers have been widely studied,[15, 16] the application of such surfaces in biomedical research remains surprisingly rare because of the often small surface coverage of the ordered areas and the poor stability of the particle layers under cell culture conditions. One recent study using single colloidal crystal (SCC) monolayers as a substrate for cell culture used Si particles of 120, 400, and 600 nm diameter which were sintered at 800˚C to promote partial coalescence between the silica microspheres and to increase the mechanical competence of the substrates.[17] The morphology of murine embryonic stem cells (mESCs) on the SCCs was more spherical compared with flat glass controls after 5 days culture. Gene and protein expression of these

spherical cells showed a similar profile to undifferentiated ESCs, suggesting the substrates not only restricted cell spreading but also subsequent differentiation. Another recent example using SCC monolayers to prevent bacterial colonization has been proposed.[18] SCCs using PS (polystyrene) colloids with sizes ranging from 220-1550 nm were deposited on PS substrates and stabilised under 95˚C for 110 min. SCCs with particle sizes in excess of 630 nm were demonstrated to prevent bacterial colonization after 24 h incubation.[18] Recently, we have developed more complex surfaces over large areas (several cm^2) composed of two colloids with ordered architectures referred to as binary colloidal crystal (BCC) layers.[10-13] The BCCs were composed of large colloids in a hexagonal arrangement with smaller colloids filling in interstitial spaces between the large colloids. The major advantage of the BCC approach is that particles of different material, size and surface chemistry can be combined, which facilitates "on-demand" design of surface topography together with multiple chemical patterns, resulting e.g. in the ability to display multiple signals to study cell-material interactions in great detail.

The aim of this study was twofold: firstly to fabricate large area, reproducible, and ordered BCC patterns with tuneable topographical feature sizes and chemistries by screening a large amount of different combinations; and secondly to demonstrate that the chosen BBC layers can be used as biomaterial substrates to control cell attachment using L929 fibroblasts, MG63 osteoblasts and primary human adipose-derived mesenchymal stem cells (hADSCs). To achieve the first goal, a screening process involving many particle combinations was undertaken to determine which BCCs could be formed. Thus, a library of BCCs with different particle sizes was generated. A systematic study screening 24 different colloid particles, including 11 large particles (≥ 1 μm) and 13 small particles (< 1 μm), made from 3 different materials, i.e. polystyrene (PS), silica (SiO_2) and poly(methyl methacrylate) (PMMA) of various size (24 nm to 5 μm) and surface functionality (unmodified, hydroxyl-, carboxylic acid- (C), amine- (N), and sulphate- (S)) was undertaken resulting in 143 BCC combinations. The surface charge of the colloidal particles as determined by zeta potential measurements and the particle size ratio and density were the clear determining factors in regard to the ability to form long-range order arrays of BCCs. The cartoon in **Figure 1** shows the fabrication of BCCs using evaporation induced confined area assembly (EICAA) as described in our previous study[10] (**Figure 1A**), and summarises the matrix of combinations and the types of colloid crystals formed (**Figure 1B**).

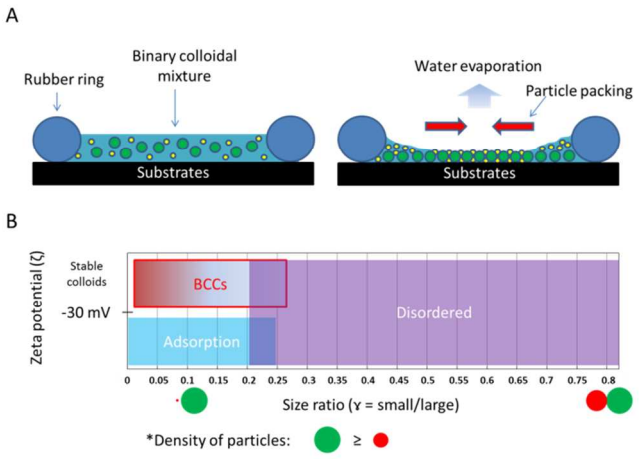

Figure 1. (A) Schematic illustration of binary colloidal crystal (BCC) formation using evaporation induced confined area assembly (EICAA). (B) Overview of the conditions needed to fabricate ordered BCCs. The critical BCC window (red square) for successful BCC formation is highlighted where particle zeta potentials (ζ) must be < -30 mV and size ratios (ɤ, small/large) < 0.2. Outside this range either disordered colloidal assemblies or aggregates, where the small particles adsorb to the surface of the large particles, are formed. Furthermore, BCCs formed large crystal areas when both particles had ζ < -30mV, the large particle had a higher density, and when ɤ was < 0.1 (red region in red box). Coatings formed under these conditions are candidates as cell culture substrates. The green and red circles on the x-axis indicate the relative size ratio of the binary colloids used in this study.

2. Experimental

2.1. Materials

Monodisperse polystyrene (PS), silica (SiO_2), and poly(methyl methacrylate) (PMMA) colloidal particles (ranging in size from 24 nm to 5 μm), bearing different functional groups (unmodified, hydroxyl-, carboxylic acid-, amine-, and sulphate-terminated) were purchased from Bangs Lab (Fishers, IN, USA), Polysciences (Warrington, PA, USA), or Invitrogen (Grand Island, NY, USA). A total of 24 colloidal particles were purchased, the details of which are listed in **Table S1**. Boron doped silicon wafers with a diameter of 10 cm, orientation <100>, and a resistivity of 1-10 Ωcm were obtained from M.M.R.C. Pty Ltd (Malvern, VIC, Australia). Absolute ethanol (AR grade) was purchased from Chem-Supply (Gillman, SA, Australia). Glass coverslips (No. 1; thickness 0.13-0.16 mm) were purchased from Marienfeld-Superior (Lauda-Königshofen, Germany).

Fibronectin (cat#F4759), phalloidin–tetramethylrhodamine B isothiocyanate (phalloidin-TRITC, cat#P1951), 4,6-diamidino-2-phenylindole (DAPI, cat#D9542), paraformaldehyde (cat#158127), bovine serum albumin (BSA, cat#A7906), monoclonal anti-Vinculin antibody produced in mouse (cat#V9131) and anti-mouse IgG (whole molecule)–FITC antibody produced in goat (cat#F2012) were purchased from Sigma-Aldrich (St. Louis, MO, USA). L929 fibroblasts (cat#CCL-1™), MG63 osteoblasts (cat#CRL-1427™), human adipose-derived mesenchymal stem cells (hADSCs, cat#PCS-500-011), Eagle's Minimum Essential Medium (EMEM, cat#30-2003) were purchased from ATCC (Manassas, VA, USA). Antibiotic–antimycotic (cat#15240-112), heat-inactivated fetal bovine serum (FBS, cat#10099-141) and sterilized phosphate buffered saline (PBS, cat#AM9625) were purchased from Invitrogen (Grand Island, NY, USA). All other reagents for cell culture and characterisation were purchased from Sigma-Aldrich (St. Louis, MO, USA) unless specified otherwise.

2.2. Preparation of binary colloidal crystals

Binary colloidal crystal (BCC) monolayers were fabricated based on evaporation induced confined area assembly (EICAA) as described previously.[13] Various combinations of binary colloidal mixtures were investigated using 24 different colloidal solutions. In each case, binary colloidal mixtures were composed of one large particle (1-5 μm in diameter, total 11 particles) and one small particle (24-820 nm in diameter, total 13 particles), resulting in a size ratio (ɤ = small/large) ranging from 0.0048 to 0.82 and a total of 143 combinations. Si wafers (1.5 x 1.5 cm) and rubber rings (1-cm-diameter) were cleaned by sonication for 15 min in ethanol twice followed by drying with a stream of nitrogen. Si wafers were then

treated with a UV-ozone cleaner (BioForce Nanoscience, Iowa, USA) for 30 min. Prior to use, colloidal solutions were fully suspended using sonication and vortexing. The amount of colloidal particles needed was calculated in advance on the basis of area encircled by the 1-cm-diameter rubber ring (~0.785 cm^2) and based on a monolayer of the large particles (**EQN S1**). For example, to produce a PS-COOH (PSC; 2 μm) and PMMA (400 nm) binary colloidal mixture inside the 1 cm diameter area, 1.99 μL PSC (2 μm; 10 wt%) and 0.24 μL PMMA (400 nm; 10 wt%) colloidal solutions were mixed and diluted in MilliQ water (pH 6.5; conductivity 0.46 μS cm^{-1}) to yield a final 100 μL mixture. The binary colloidal mixture was carefully pipetted inside the confined area encircled by the rubber ring. The samples were kept at room temperature until complete evaporation of the solvent.

2.3. Substrate and particle characterisation

The top-view structure of BCC monolayers was observed using field emission scanning electron microscopy (FE-SEM; ZEISS SUPRA 40 VP, Carl Zeiss, Germany) at 3-5 keV. Prior to image capture, samples were coated with 20 nm Au using evaporation. Surface coverage and BCC percentage was quantified from SEM images. Surface coverage and BCC percentage of each combination were judged into three categories: high (> 70%), medium (70%-40%), and low (< 40%). The zeta potential of colloids was measured using a Zetasizer Nano ZSP instrument (Malvern Instruments, UK). Analysis was carried out following the supplier's instructions. Briefly, colloidal solutions were diluted to 0.05 wt% using MilliQ water (pH 6.5). Subsequently, the colloidal solutions (0.6 mL) were transferred in a disposable capillary cell. The zeta potential of each colloidal solution was averaged from thirty data points (n = 30). The zeta potential of substrates was measured using a SurPASS electrokinetic analyser (Anton Paar, Austria). Analysis was carried out following the supplier's instructions. Briefly, substrates with a size of 55 mm x 25 mm were treated with ozone and analysed using a clamping cell. The zeta potential of each substrate was measured using 10 mM $MgCl_2$. Zeta potential values were averaged from ten data points (n = 10). Surface wettability of BCC monolayers was determined using sessile drop water contact angle (WCA) measurements (KSV instruments Ltd, Finland). The WCA was measured in each case using 1 μL MilliQ water on 5 samples for each BCC monolayer (n = 5) using a WCA goniometer (FTA-125, First Ten Ångstroms, USA). The surface roughness was determined using atomic force microscope (AFM, Dimension iCon, Bruker Corp., Billerica, MA, USA). Three samples (n = 3) were scanned using ScanAsyst mode with a scan rate of 0.75 Hz and a scan area of 20 x 20 um^2.

2.4. Cell culture

Four types of BCC monolayers (5 μm Si/0.4 μm PMMA (Si5PMMA04), 5 μm Si/0.4 μm PSC (Si5PSC04), 2 μm Si/0.11 μm PMMA (Si2PMMA011), and 2 μm Si/0.22 μm PSC (Si2PSC022)) were chosen for cell culture experiments. BCC monolayers were stabilised using heat treatment (200 °C for 60 sec) to melt the small particles. Small polymer particles acted as a glue to immobilise the entire BCC layer. Before cell seeding, substrates were sterilised with 1% antibiotic–antimycotic/PBS for 30 min and then rinsed with PBS three times. Fibronectin adsorption was carried out at 100 μg/mL for 1 h at room temperature followed by rinsing with MilliQ water twice. L929 fibroblasts, MG63 osteoblasts and human adipose-derived mesenchymal stem cells (hADSCs) were cultured according to the supplier's instructions. In this study, fibroblasts and osteoblasts before passage 30 and hADSCs before passage 6 were used exclusively. Cell attachment and spreading on BCC monolayers and two flat controls (Si wafers, SiO_2, and tissue culture polystyrene, TCPS) were studied after 24 h. Briefly, cells were fixed by 4% (v/v) paraformaldehyde/PBS for 10 min, permeabilized by 0.1% (v/v) Triton-X100/PBS for 15 min, and then blocked with 1% (w/v) bovine serum albumin/PBS for 30 min. The samples were then incubated with the monoclonal mouse anti-vinculin antibody (1:100 dilution in PBS) at room temperature for 1 h followed by incubation with FITC-labelled anti-mouse-IgG antibodies (1:100 dilution in PBS) at room temperature for 1 h. F-actin and nuclei were stained with phalloidin–TRITC (500 nM in PBS) and DAPI (100 nM in PBS) for 1 h, respectively. Fluorescent images were captured using inverted Epi-fluorescence microscopy (Eclipse Ti-E, Nikon Instruments Inc., Japan). For SEM observations, samples were dehydrated in a series of ethanol solutions from 50-100%, dried in air, and then coated with 20 nm Au. Cell density and spreading area were quantified automatically using NHS ImageJ software according to the software instructions. Cell density and cell spreading area was analysed using six images per sample (n = 6). Data were expressed as mean±standard error mean (SEM) when the analyzed sample number was different and as mean±standard deviation (STDEV) when the analyzed sample number was the same. Statistical analysis was performed using GraphPad Instat 3.0 (GraphPad Software, La Jolla, CA, USA). The statistical analysis between each group was determined with one-way ANOVA and Student–Newman–Keuls multiple comparison tests. $p < 0.05$ was considered a significant difference.

3. Results and discussion

3.1. Binary colloidal crystal monolayers

The ability to form ordered BCCs can be described by the forces of interaction that take place between the two particles, the particles and the substrate surface, and the solvent they are suspended in. DLVO theory best describes the electrostatics involved in the assembly process,[19] however capillary, depletion and entropic forces also have been described as key factors playing a role in BCC formation. The role of these forces affecting BCC formation has been discussed in detail in our previous studies.[10-13] Here, we report the new finding of BCC formation based on a real time observation technique, and focus on the fabrication of BCC layers covering large areas for biological applications. From 143 particle combinations, we found that at least 44 can form BCC structures (**Figure 2**). These combinations cover a wide range of size ratios (γ), ranging from 0.005 to 0.27, and can only form when both particles are negatively charged with zeta potentials (ζ) smaller than -30 mV. **Figure 3** shows all particle zeta potential data and negatively charged substrates (e.g. glass slides, Si wafers, and PS slides after ozone treatment). To form large area BCC layers, the density of particles and wettability of substrates were also crucial. Firstly, the density of particles determines whether BCCs form in three-dimensions (3D) first or if a 2D array forms on the surface directly (**Figure 4**). When large Si particles are mixed with small polymer particles (representing different densities), the Si particles settle down on the surface at an early stage and form a loosely packed 2D layer. The suspended small polymer particles subsequently settle on the surface and fill the voids between the Si particles in the final packing stages to form close-packed BCC layers. On the other hand, when two polymer particles (representing similar densities) are mixed, matched particle-particle interactions lead to BCC formation in suspension. These 3D BCCs settle down on the surface due to gravitational forces or when the solvent volume gets diminished and

spread out forming 2D crystals. In this case, BCCs distributed randomly on the surface resulting in separated crystal islands and lower surface coverage. On the contrary, large polymer particles mixed with small Si particles cannot form BCCs due to sedimentation of small particles at an early stage (e.g. combination 36: 2 µm PSS and 0.3 µm Si particles (PSS2-Si03) in **Table S1**). Secondly, hydrophilic surfaces were more efficient at facilitating particle packing when the water contact angle (WCA) was below 20˚ (after ozone treatment, WCA of glass slides: 5˚±1˚; Si wafers: 3˚±1˚; and PS slides: 20˚±4˚), although smaller areas of BCC structures could be found on hydrophobic surfaces (before ozone treatment). Based on the desired cell culture application, a large BCC area (> 1 mm^2) was desired. High quality BCC structures were found when the size ratio was in a narrow range of 0.02-0.1 within the BCC window. Outside this range, only BCCs with small surface coverage were found. In summary, successful BCC formation over large areas occurs on hydrophilic and negatively charged substrate surfaces when using two stable negatively charged colloids (e.g. large Si particles and small polymer particles) with a size ratio ranging from 0.02-0.1 (**Figure 1B**).

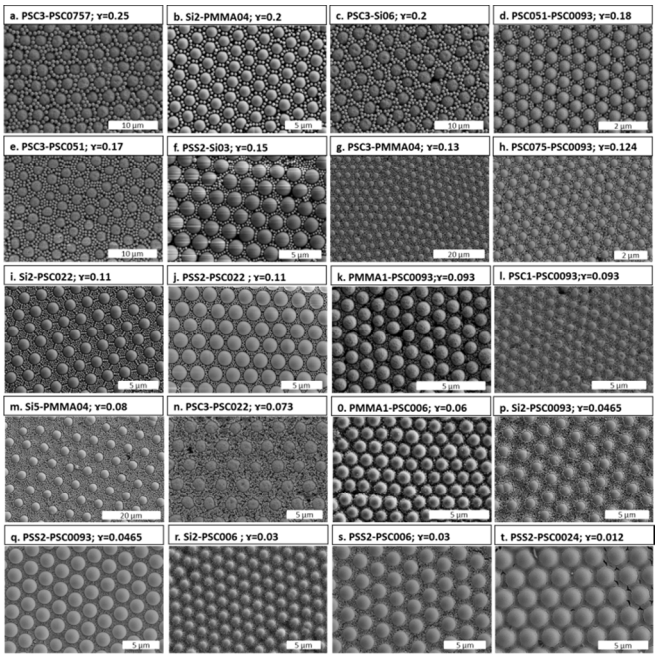

Figure 2. Binary colloidal crystal (BCC) layers. Selected images show different size ratios (γ) ranging from 0.012-0.25. In each case, the sample description indicates the large particle/small particle type and size (in µm) used and also provides the particle size ratio (γ). All particles used had a zeta potential < -30 mV. PSC: carboxylated polystyrene; PSN: aminated polystyrene; PSS: sulphated polystyrene; PMMA: poly(methyl methacrylate); SiC: carboxylated silica; SiN: aminated silica.

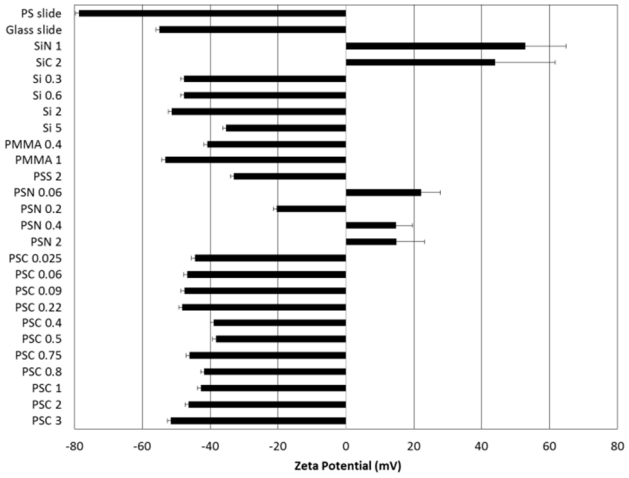

Figure 3. Zeta potentials of the colloidal particles and substrates (PS and glass slides). Si wafers have a large negative zeta potential (-412±63 mV) due to it semiconductivity. Y-axis indicates colloidal material and size. For example, SiN 1 indicates an aminated silica particle with a diameter of 1 µm. PS: polystyrene; PSC: carboxylated polystyrene; PSN: aminated polystyrene; PSS: sulphated polystyrene; PMMA: polymethyl methacrylate; Si: silica; SiC: carboxylated silica; SiN: aminated silica. Two flat substrates, PS and glass slides, were ozone-treated. Values = mean±STDEV (n = 30 for colloids and n = 10 for substrates).

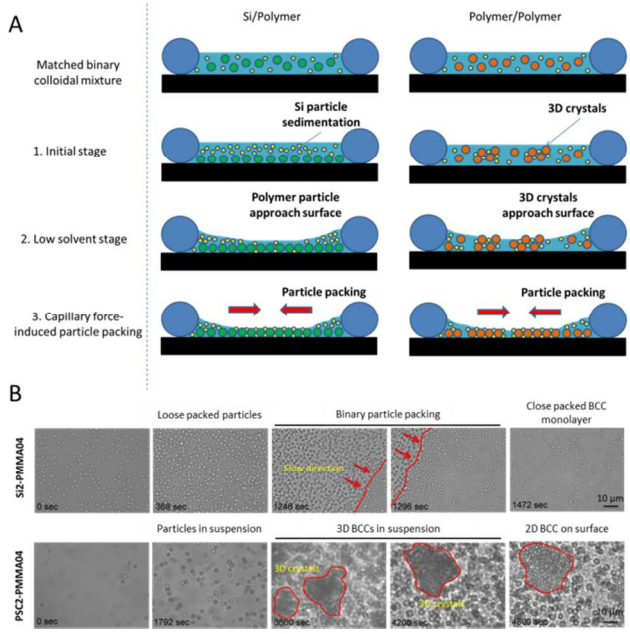

Figure 4. (A) Schematic illustration of BCC formation depending on different particle densities. The left hand column describes large Si particles mixed with small polymer particles (Si/Polymer), whilst the right hand column describes two polymer particles (Polymer/Polymer). BCC formation using evaporation induced confined area assembly (EICAA) can be distinguished into three stages: 1) initial stage where sedimentation happens for Si particles, whilst polymer particles interact with each other in suspension; 2) low solvent stage where a monolayer of Si particles formed, whilst 3D polymer crystals found on the surface; 3) capillary force induced particle packing where the Si particles form hexagonal close packed structures with small particles filling in the voids, whilst 3D crystals are spread out on the surface and the rest of particles fill in the space to connect those forming 2D crystals. While the Si/polymer generates a large surface coverage of BCC, the crystals of polymer/polymer particles is smaller and

disconnected. (B) Two examples represent the illustration above. Real time images were captured using an inverted optical microscopy equipped with superfast (1 ms) time lapse recording function.

From the 44 BCC structures, we found that for some combinations with the same size ratio, the arrangement of small particles is different (i.e. 2 μm Si and 0.22 μm PSC particles (Si2-PSC022, image i) vs. 2 μm PSS and 0.22 μm PSC particles (PSS2-PSC022, image j), γ = 0.11, **Figure 2**). In this case, three small particles assemble in a line in between two large particles in the Si2-PSC022 crystal, whilst only one small particle is observed between two large particles in the PSS2-PSC022 crystal. Similar observations were made with Si2-PSC0093 and PSS2-PSC0093 (γ = 0.0465, image p vs. q, **Figure 2**). We also noticed that for the latter combination of PSS2-PSC0093, the small PSC0093 particles accumulate on the surface of the large Si2 particles. This phenomenon was also found in other combinations, e.g. PSC3-PSC022 (γ = 0.073, image m), Si2-PSC0093 (γ = 0.0465, image p), and Si2-PSC006 (γ = 0.03, image r, **Figure 2**), suggesting that subtle differences between combinations will change the BCC structure as seen from SEM images.

For other combinations outside the window of size ratio and zeta potential, two types of random structures were formed during particle self-assembly: disordered structures and aggregates (assemblies with smaller particles adsorbed to the surface of the larger particles). Disordered structures were formed with 55 combinations having size ratios ranging from 0.15 to 0.82 (**Figure S1A).** There were 44 combinations showing particle-particle adsorption in the size ratio ranging from 0.0048 to 0.22 (**Figure S1B),** which included particles having the same surface charge. Both the disordered structure and particle adsorption was mainly due to a mismatch of zeta potential and size ratio of particles. It is reasonable to assume that particle adsorption occurred when the particle charge was opposite. However, when two particles with the same charge were mixed but one of these had a low zeta potential, particle adsorption also occurred. These unstable particles not only attract each other, but also stick to the substrate surface, resulting in either particle adsorption or disordered particle assemblies. When the size ratio is small, particle adsorption tends to happen. On the other hand, disordered structures were found when the size ratio was large. However, particle adsorption also appeared to be size ratio dependent if the size ratio is smaller than 0.012 (i.e. the difference in diameter is greater than 50 times).

In order to study the potential of using BCCs as cell culture substrates we selected crystals that demonstrated a high frequency of BCC structure. These included the following combinations: 5 μm Si/0.4 μm PSC (Si5-PSC04), 5 μm Si/0.4 μm PMMA (Si5-PMMA04), 2 μm Si/0.22 μm PSC (Si2-PSC022), and 2 μm Si/0.11 μm PMMA (Si2-PMMA011). The selected BBC layers had surface coverages of at least 70% of BCC structures over the entire surface (**Figure 5**). Prior to cell seeding, substrates were heat treated at 200 ˚C for 1 min to stabilise the BCC layers by melting the small polymer colloids. The conditions needed to melt polymer colloids are more gentle than that those needed to sinter Si particles (800 ˚C for 3 h).[17] Surface properties were determined before cell culture using atomic force microscopy (AFM) and water contact angle (WCA) measurements (**Table 1**). The surface roughness of BCCs ranged from 92 nm to 267 nm, and the WCA of the BCCs ranged from 43˚ to 84˚ depending on the combinations (**Table 1**). The ability of these BCCs to modulate cell morphology, spreading, and attachment was investigated using three different cell types (fibroblasts, osteoblast, and hADSCs) in 24 h cell culture experiments. In addition, because extracellular matrix (ECM) proteins such as fibronectin (FN) and its cell binding domain, Arg–Gly–Asp (RGD) sequence, are known to have a dramatic influence on the cellular response to artificial topographies,[20] the role of a uniform layer of FN adsorbed to the BCCs was also studied.

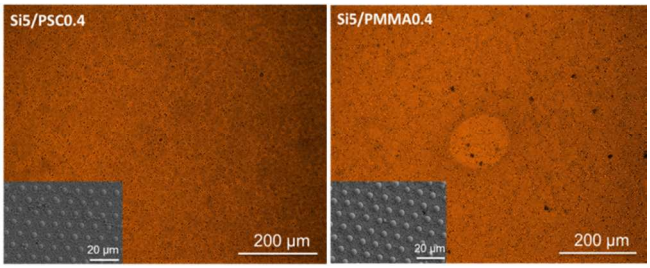

Figure 5. Optical images of large surface areas displaying BCC structure. Two examples of Si5PSC04 and Si5PMMA04 show a large surface area (~ 1 mm^2) covered by BCCs. SEM image insets show the detail structure accordingly.

Table 1. Surface characterization data of four BCC layers used in cell culture experiments. Water contact angles (WCAs) were measured using 0.5 μL MilliQ water on 5 samples for each BCC monolayer (n = 5). Surface roughness (Ra) was determined from three samples (n = 3) with an area of 20 x 20 μm^2. Values = mean±STDEV.

	Si5PSC04	Si5PMMA04	Si2PSC022	Si2PMMA011
Ra (nm)	267.6±16.5	180.1±4.9	103.6±3.2	92.1±4.1
WCA (˚)	83.9±2.7	59.4±3.7	43.6±1.8	53.5±0.6

3.2. Cell culture

In cell culture experiments the morphology of hADSCs was fully spread out on flat Si wafers and TCPS but elongated on Si5-PSC04 (**Figure 6a-d**). In addition, the amount of filopodia and protrusions were decreased after attachment to BCCs compared with flat surfaces. Statistically, the cell spreading area of hADSCs on TCPS (5210±523 μm^2) was larger than that on BCCs (Si5-PSC04: 2840±133 μm^2, Si5-PMMA04: 3176±431 μm^2, Si2-PSC022: 2774±835 μm^2, and Si2-PMMA011: 2499±452 μm^2, $p < 0.01$) and Si wafers (Si wafer: 3582±447 μm^2, $p < 0.05$, **Figure 6g**). Vinculin staining further showed that clear focal adhesions and stretched F-actin was found on the Si wafers, but not on the Si5-PSC04 (**Figure 6h**), suggesting a weaker adhesive force and cytoskeletal tension of cells on BCC substrates. After FN coating, the cell spreading area on Si and BCCs was comparable to TCPS (Si wafer-Fn: 6051±292 μm^2, and Si5-PMMA04-Fn: 5185±408 μm^2, **Figure 6g**). It suggested that both surface topography and cell adhesive protein presentation are important for stem cell adhesion. In general, the trend of the adhesion of osteoblasts and fibroblasts on BCCs and flat controls was similar to the hADSCs with subtle differences (**Figure 7**), suggesting that the topography effect is cell-type dependent but the overall trend toward the same conclusion that BCCs inhibit cell spreading.

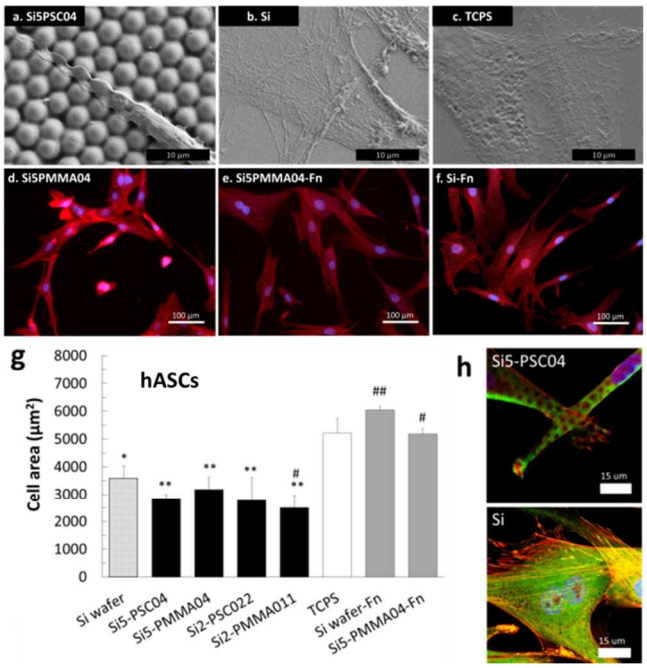

Figure 6. Human adipose-derived mesenchymal stem cells (hADSCs) on BCC substrates that were heat treated prior to cell culture. (a-c) Scanning electron micrographs (SEMs) of cells on (a) Si5PSC04, (b) Si wafer, and (c) TCPS. (d-f) Fluorescence micrographs of cells on (d) Si5PMMA04, (e) Fn-coated Si5PMMA04 (Si5PMMA04-Fn), and (f) Fn-coated Si wafer (Si wafer-Fn) surfaces. F-actin (red) and nucleus (blue) was stained. (g) Cell spreading area on various surfaces. Value = mean ± standard error mean (n = 113-132). * and # indicates that there is a significant difference versus TCPS and Si wafer, respectively. One, two and three symbols indicate $p < 0.05$, 0.01, and 0.001, respectively. (h) Confocal micrographs of cells on Si5-PSC04 and Si wafer. Vinculin (green), F-actin (red) and nucleus (blue) were stained.

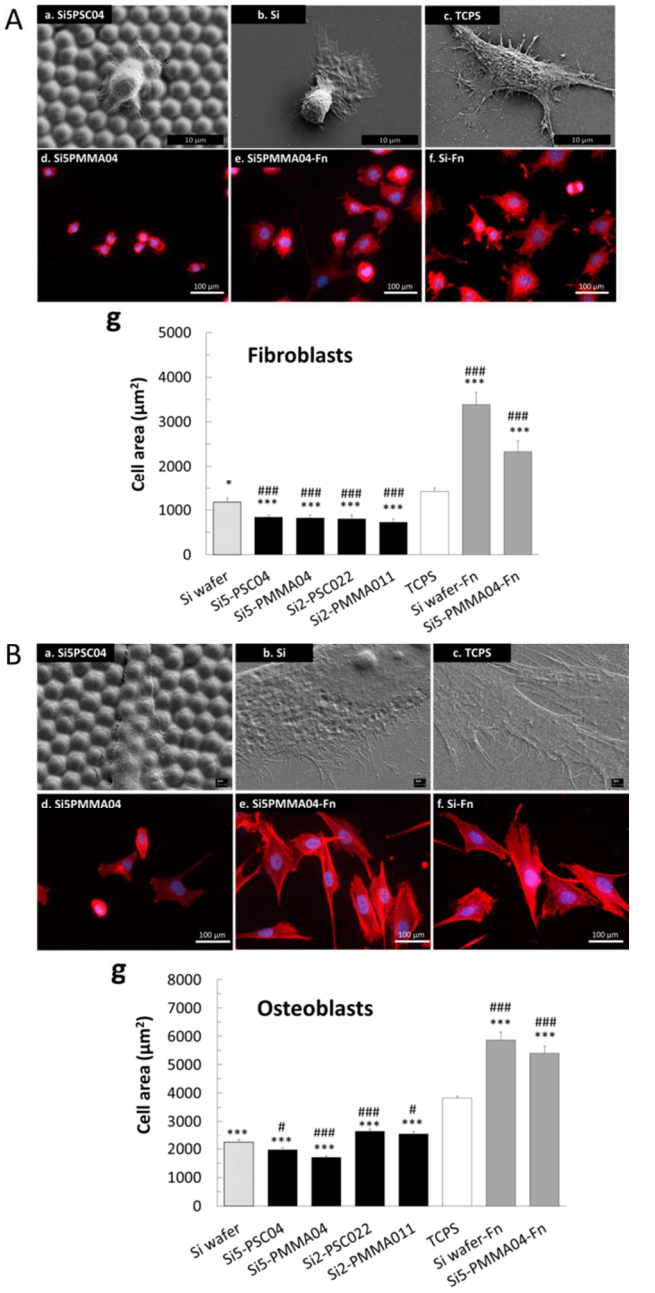

Figure 7. (A) L929 fibroblast and (B) MG63 osteoblast attachment and spreading on BCC substrates that were heat treated prior to cell culture. (a-c) Scanning electron micrographs (SEMs) of cells on (a) Si5PSC04, (b) Si wafer, and (c) TCPS. (d-f) Fluorescence micrographs of cells on (d) Si5PMMA04, (e) Fn-coated Si5PMMA04 (Si5PMMA04-Fn), and (f) Fn-coated Si wafer (Si wafer-Fn) surfaces. F-actin (red) and nucleus (blue) was stained. (g) Cell spreading area on various surfaces. Values = mean ± standard error mean (n = 291-422). * and # indicates that there is a significant difference versus TCPS and the Si wafer substrate, respectively. One, two and three symbols indicate $p < 0.05$, 0.01, and 0.001, respectively.

These preliminary cell culture experiments using BCCs show several important outcomes. Firstly, cell spreading was inhibited on BCCs compared with flat substrates, whilst cell attachment density was not influenced to the same extent by BCCs in comparison to flat surfaces, except in the case of osteoblasts (**Figure S2**). Secondly, the degree of cell spreading inhibition was

BCC combination and cell type dependent. Lastly, the FN coating significantly increased cell spreading of all three cell types but with varying degrees; FN increased the cell attachment density of only osteoblasts (**Figure S2**), and increased the nucleus area (~2-fold) of only fibroblasts (**Figure S3**). This suggests that cells chosen for specific purposes will need to be investigated on BCC substrates of a given morphology as there are no general rules that can be made regarding the responses of the different cell types to these new substrates. Therefore, when developing new substrates to control cell behaviour it is important to compare different cell types.

Cellular responses to biomaterial surfaces can be correlated to surface roughness, surface chemistry, and substrate stiffness.[21-24] On selected BCC monolayers, the surface is composed of Si particles with a polymer glue in between Si particles overall providing a substrate that can be seen as a "bumpy surface" with an ordered chemical pattern (Si/polymer pattern). Cell spreading is larger on TCPS (PS-COOH) than Si wafers (SiO_2), suggesting that an embedded PS in BCCs should improve the adhesion and spreading in terms of chemical effects. However, the averaged cell area on BCCs is even lower than Si wafers, suggesting that these 'bumpy surfaces' with surface roughnesses in the hundred nanometers range (Ra ~ 100-300 nm) are efficient and can be used to inhibit cell spreading even if a cytophilic polymer is embedded. Nevertheless, surface chemistry does play a role to compensate the topography effect resulting in a low but significance between Si wafer and BCCs (Si/polymer). To further study the topographic and chemical effect, fibroblasts were culture on SCCs and BCCs (Figure S4). While fibroblasts were elongated on SCC (PS-COOH) monolayers, cell morphology became rounded after embedding small PMMA particles into the monolayer forming a BCC layer. It suggests that the complexity of BCCs can tune cell behaviour using various particle combinations although the overall surface effect is still cell-type dependent. We also found that the thin and long cell protrusions often observed on flat surfaces are significantly decreased, and that filopodia are shortened or not present for all three cell types on BCCs. A smaller cell spreading area with less visible filopodia and less numbers of focal adhesions often indicates a weaker adhesion force and/or less tension on the cytoskeleton.[25] These changes have been reported to have the potential to alter the cell fate directly from morphological change or indirectly from intracellular signal cascades,[26-29] and the BCC substrates provide an opportunity to vary the cellular microenvironment in a rapid way to investigate these processes.

A number of techniques have been developed for fabricating surface nanotopographies for mammalian cell culture experiments.[30] The data generated in this study however demonstrate several important issues relating to the use of ordered binary particle layers in mammalian cell culture. Firstly, the ability to fabricate ordered surface nanotopographies using a simple and cost effective method highlights their potential as a tool for cell culture studies. Secondly, the use of mixed particle systems of different size with heterogeneous chemistries opens up possibilities to probe the role played by controlled ligand spacing and concentration, and controllable topographies on cellular processes. Lastly, there are clear differences in the behaviour of three cells types induced by the BCCs opening up the possibility for tailoring surface structure/morphology depending on the application. Furthermore, two possibilities exist for decorating the colloid crystals with bioactive moieties. 1) Pre-coating particles with proteins or peptides prior to assembly as we have previously demonstrated[10] or 2) use of different particle chemistries to selectively immobilise biomolecules such as integrin-binding peptides after colloidal assembly thus turning the surfaces into multi-signal surfaces presenting both topographical and chemical cues in an ordered architecture. In addition, we have shown that colloidal crystals with up to four particles are possible,[11] again with different chemistries, thus opening up the possibility of having even more complex surfaces to probe cellular responses. This is a differentiating factor of BCCs and more complex crystals compared to using SCCs which have been used for embryonic stem cell culture.[17] An added advantage is the ability to stabilise the assembled structures with polymeric particles, where for example the small particles act as a glue to stabilise the crystal by partial melting. Finally, compared to lithography methods such as e-beam lithography, BCCs are easy to access at low cost.[6]

4. Conclusions

In conclusion, we established a library for the formation of various combinations for BCC layers, fabricated a novel family of substrates with well-defined surface topography and chemistry with large-area coverage, and demonstrated that these can be exploited as a tool to study and control cellular responses. The preliminary cell culture experiments with fibroblasts, osteoblasts and hADSCs shows that the cell spreading can be inhibited on the BCCs due to the topographic effects while the surface chemistry could compensate this effect in some circumstances. In regard to future research, control of cell spreading is of interest in stem cell related research, and here more specifically in the culture of ESCs or induced pluripotent stem cells (iPSCs). For example, ESCs tend to keep their pluripotency in rounded morphology during *in vitro* culture. Topographic and chemical effects on stem cell differentiation occur via different pathways.[2] Using biomaterial surfaces with optimized surface topography and chemistry to modulate stem cell growth or differentiation has the potential to provide easier, more controlled culture protocols at reduced cost.

Acknowledgements

The Scientific Industrial Endowment Fund (SIEF) is acknowledged for providing a John Stocker Postdoctoral Research Fellowship for PYW. Swinburne University of Technology is acknowledged for a SUPRA PhD Scholarship for PKo and CSIRO is acknowledged for funding PKo through an OCE Science Team postgraduate scholarship. The Australian Research Council is acknowledged for funding a PhD scholarship for HP through the Discovery Program (ARC-DP). This work was performed in part at both the Biointerface Engineering Hub @Swinburne and MCN as part of the Victorian Node of the Australian National Fabrication Facility, a company established under the National Collaborative Research Infrastructure Strategy to provide nano and microfabrication facilities for Australia's researchers.

Notes and references

[a] Swinburne University of Technology, Industrial Research Institute Swinburne (IRIS), and Department of Chemistry and Biotechnology, Hawthorn, 3122 VIC, Australia. *E-mail: pkingshott@swin.edu.au

[b] CSIRO Manufacturing Flagship, Bayview Avenue, Clayton, 3168 VIC, Australia

Electronic Supplementary Information (ESI) available: Two tables and four figures can be found in the Supporting Information which is available from the Online Library or from the author. See DOI: 10.1039/c000000x/

1. P. Koegler, A. Clayton, H. Thissen, G. N. Santos and P. Kingshott, *Adv Drug Deliv Rev*, 2012, **64**, 1820-1839.
2. M. J. Dalby, N. Gadegaard, R. Tare, A. Andar, M. O. Riehle, P. Herzyk, C. D. W. Wilkinson and R. O. C. Oreffo, *Nature materials*, 2007, **6**, 997-1003.
3. C. J. Bettinger, R. Langer and J. T. Borenstein, *Angew Chem Int Edit*, 2009, **48**, 5406-5415.
4. S. Turunen, A. M. Haaparanta, R. Aanismaa and M. Kellomaki, *J Tissue Eng Regen M*, 2013, **7**, 253-270.
5. J. Norman and T. Desai, *Ann Biomed Eng*, 2006, **34**, 89-101.
6. M. A. Wood, *J R Soc Interface*, 2007, **4**, 1-17.
7. P.-Y. Wang, T.-H. Wu, P.-H. Chao, W.-H. Kuo, M.-J. Wang, C.-C. Hsu and W.-B. Tsai, *Biotechnol Bioeng*, 2013, **110**, 327-337.
8. P.-Y. Wang, H.-T. Yu and W.-B. Tsai, *Biotechnol Bioeng*, 2010, **106**, 285-294.
9. S. Y. Chou, P. R. Krauss and P. J. Renstrom, *Appl Phys Lett*, 1995, **67**, 3114-3116.
10. G. Singh, S. Pillai, A. Arpanaei and P. Kingshott, *Adv Mater*, 2011, **23**, 1519-1523.
11. G. Singh, H. J. Griesser, K. Bremmell and P. Kingshott, *Adv Funct Mater*, 2011, **21**, 540-546.
12. G. Singh, S. Pillai, A. Arpanaei and P. Kingshott, *Adv Funct Mater*, 2011, **21**, 2556-2563.
13. G. Singh, S. Pillai, A. Arpanaei and P. Kingshott, *Soft Matter*, 2011, **7**, 3290-3294.
14. X. Z. Ye and L. M. Qi, *Nano Today*, 2011, **6**, 608-631.
15. Y. Li, G. T. Duan, G. Q. Liu and W. P. Cai, *Chem Soc Rev*, 2013, **42**, 3614-3627.
16. Z. F. Dai, Y. Li, G. T. Duan, L. C. Jia and W. P. Cai, *Acs Nano*, 2012, **6**, 6706-6716.
17. L. J. Ji, V. L. S. LaPointe, N. D. Evans and M. M. Stevens, *Eur Cells Mater*, 2012, **23**, 135-146.
18. M. Kargar, A. Pruden and W. A. Ducker, *J Mater Chem B*, 2014, **2**, 5962-5971.
19. E. J. W. Verwey, *J Phys Colloid Chem*, 1947, **51**, 631-636.
20. C. Gonzalez-Garcia, S. R. Sousa, D. Moratal, P. Rico and M. Salmeron-Sanchez, *Colloids Surf B Biointerfaces*, 2010, **77**, 181-190.
21. P.-Y. Wang, L. R. Clements, H. Thissen, A. Jane, W.-B. Tsai and N. H. Voelcker, *Adv Funct Mater*, 2012, **22**, 3414-3423.
22. P. Y. Wang, W. B. Tsai and N. H. Voelcker, *Acta Biomater*, 2012, **8**, 519-530.
23. P. Y. Wang, L. R. Clements, H. Thissen, W. B. Tsai and N. H. Voelcker, *Acta biomaterialia*, 2015, **11**, 58-67.
24. P.-Y. Wang, J. Yu, J.-H. Lin and W.-B. Tsai, *Acta biomaterialia*, 2011, **7**, 3285-3293.
25. X. S. Liu, H. J. Luo, H. Yang, L. Wang, H. Kong, Y. E. Jin, F. Wang, M. M. Gu, Z. Chen, Z. Y. Lu and Z. G. Wang, *J Cell Biochem*, 2007, **100**, 1288-1300.
26. D. Hong, H. X. Chen, H. Q. Yu, Y. Liang, C. Wang, Q. Q. Lian, H. T. Deng and R. S. Ge, *Exp Cell Res*, 2010, **316**, 2291-2300.
27. F. Li, B. Li, Q. M. Wang and J. H. Wang, *Cell Motil Cytoskel*, 2008, **65**, 332-341.
28. E. K. F. Yim and M. P. Sheetz, *Stem Cell Res Ther*, 2012, **3**.
29. M. Ventre, F. Causa and P. A. Netti, *J R Soc Interface*, 2012, **9**, 2017-2032.
30. K. Anselme and M. Bigerelle, *Int Mater Rev*, 2011, **56**, 243-266.

The table of contents

Large-area highly ordered self-assembled binary colloidal crystal (BCC) monolayers are fabricated for mammalian cell culture and biointerface control.

Keywords: binary colloidal crystal, self-assembly, human mesenchymal stem cells, surface chemistry, surface topography

Peng-Yuan Wang, Hitesh Pingle, Peter Koegler, Helmut Thissen, and Peter Kingshott*

Title: Self-assembled binary colloidal crystal monolayers as cell culture substrates

ToC figure